HHS Public Access

Author manuscript

*Nat Chem Biol*. Author manuscript; available in PMC 2019 May 02.

Published in final edited form as:

*Nat Chem Biol*. 2018 September ; 14(9): 870–875. doi:10.1038/s41589-018-0105-5.

# Designed peptides that assemble into cross-α amyloid-like structures

**Shao-Qing Zhang**[1,2,3], **Hai Huang**[3,7], **Junjiao Yang**[2,3,7], **Huong T. Kratochvil**[2,3], **Marco Lolicato**[3], **Yanxin Liu**[4], **Xiaokun Shu**[2,3], **Lijun Liu**[3,5], and **William F. DeGrado**[2,3,6]

[1]Department of Chemistry, University of Pennsylvania, Philadelphia, PA, USA.

[2]Department of Pharmaceutical Chemistry, University of California at San Francisco, San Francisco, CA, USA.

[3]Cardiovascular Research Institute, University of California at San Francisco, San Francisco, CA, USA.

[4]Department of Biochemistry and Biophysics, University of California at San Francisco, San Francisco, CA, USA.

[5]DLX Scientific, Lawrence, KS, USA.

[6]Institute for Neurodegenerative Diseases, University of California at San Francisco, San Francisco, CA, USA.

[7]These authors contributed equally: Hai Huang, Junjiao Yang.

## Abstract

Amyloids adopt 'cross-β' structures composed of long, twisted fibrils with β-strands running perpendicular to the fibril axis. Recently, a toxic peptide was proposed to form amyloid-like cross-α structures in solution, with a planar bilayer-like assembly observed in the crystal structure. Here we crystallographically characterize designed peptides that assemble into spiraling cross-α amyloid-like structures, which resemble twisted β-amyloid fibrils. The peptides form helical dimers, stabilized by packing of small and apolar residues, and the dimers further assemble into

**Correspondence and requests for materials** should be addressed to X.S. or L.L. or W.F.D.
*xiaokun.shu@ucsf.edu; lijunliuks@gmail.com; william.degrado@ucsf.edu

author contributions

S.-Q.Z. and W.F.D. conceived the project. S.-Q.Z. designed all the peptide sequences and performed in vitro experiments with H.T.K., M.L. and Y.L. H.H. and J.Y. conducted cellular in vivo experiments. L.L. solved and refined all the crystal structures. S.-Q.Z., H.H, J.Y., H.T.K., Y.L., X.S., L.L. and W.F.D. analyzed the data. S.-Q.Z. and W.F.D. prepared the manuscript with contributions from all the authors.

**Supplementary information** is available for this paper at https://doi.org/10.1038/s41589-018-0105-5.

**Reprints and permissions information** is available at www.nature.com/reprints.

Methods

Methods, including statements of data availability and any associated accession codes and references, are available at https://doi.org/10.1038/s41589-018-0105-5.

**Data availability.** The crystal structures of $\alpha Am_{mem}$, $\alpha Am_G$, $\alpha Am_G$ (low resolution), αAms, $\alpha Am_L$ and αTet have been deposited in the RCSB Protein Database Bank under the codes 6C4X, 6C4% 6C4Z, 6C50, 6C51 and 6C52, respectively. An additional crystalline form of αAmL has been deposited under the PDB code 6D02. The data sets in the current study are also available from the corresponding authors upon request.

Competing interests

The authors declare no competing interests.

cross-a amyloid-like fibrils with superhelical pitches ranging from 170Å to 200Å. When a small residue that appeared critical for packing was converted to leucine, it resulted in structural rearrangement to a helical polymer. Fluorescently tagged versions of the designed peptides form puncta in mammalian cells, which recover from photobleaching with markedly different kinetics. These structural folds could be potentially useful for directing in vivo protein assemblies with predetermined spacing and stabilities.

## Reporting Summary.

Further information on experimental design is available in the Nature Research Reporting Summary linked to this article.

---

Understanding the principles by which peptides organize into higher-order assemblies is a topic of considerable interest in the soft matter, biological and chemical communities[1]. The emerging principles inform our knowledge of normal and pathological processes in biology, and this knowledge is translating to the construction of soft materials with diverse functions, including stimulus-responsive hydrogel sensors[2] and vehicles for drug delivery[3]. In particular, the study of β-amyloids[4] represents a large area of science, with implications for understanding neurodegeneration[5], amyloid diseases[6] and epigenetic phenomena[7]. β-Amyloids have also been widely used to design nanomaterials[8] and catalysts[9–11]; they also are proposed to represent key steps in the molecular evolution of proteins[12,13]. Classically, amyloids have 'cross-β' structures, in which the β-strands align perpendicular to the long axis of an infinite fibril. By contrast, in self-assembling elongated helical peptides such as coiled coils, the helices generally align nearly parallel to the fiber axis. Therefore, it was surprising to discover that a toxic peptide, PSMα3, from *Staphylococcus aureus* formed cross-α amyloid-like structures in which the helices were proposed to align perpendicular rather than parallel to the fibril axis[14]. The assembly was demonstrated by negative-stain electron microscopy (EM) and the ability to bind an amyloid-staining dye. Furthermore, the peptide crystallized in a bilayer-like arrangement with the helices interacting laterally. Prior to this work, designed peptides had been found to crystallize as bilayers[15,16], but the same peptides did not appear to form fibrils in solution.

Given that the cross-α structure has only recently been proposed as an important organizing principle in nature, very little is known about the general physical principles by which cross-α amyloid-like structures form or the extent to which the morphology of the cross-α amyloid-like structures can be manipulated by design. Peptide nanotubes have been designed on the basis of a coiled-coil repeat, which aligned either perpendicular or diagonal to the long axis of the tube, as seen by EM at near-atomic resolution[17]. Additionally, a number of repeat proteins that incorporate loops between helices have been prepared[18–20]. Nevertheless, structures of self-assembling spiraling cross-α amyloid-like structures have yet to be observed.

Here, we describe the structure of a membrane-interactive peptide that surprisingly forms a long, twisted cross-α spiral. We then analyze the structural features stabilizing the spiral to guide the design of water-soluble cross-α amyloid-like structures that assemble in vitro and in vivo. Finally, we demonstrate how small sequence changes can translate into large

changes in the supramolecular structure and how these structural changes influence their ability to assemble and remodel within living cells.

## Results

### X-ray structure of a cross-α spiral hydrophobic peptide.

Our discovery of a structurally well-defined cross-α structure arose from a serendipitous discovery of the packing in the crystal structure of $\alpha Am_{mem}$, an analog of the membrane-spanning $Zn^{2+}$-transporting peptide Rocker[21] based on the backbone of a mononuclear $Zn^{2+}$- binding four-helix bundle[22] (Supplementary Fig. 1a). $\alpha Am_{mem}$ adopted an antiparallel dimer of straight α-helices, which further assembled into long counter-clockwise twisted fibrils in the crystal lattice (Supplementary Fig. 1b). Similarly to cross-β structures, the axes of the α-helices lie perpendicular to the main superhelical axis of this structure (Fig. 1a). The superhelix is formed from secondary structural units that interact across the fibril axis to create a two-layered structure, as shown in Fig. 1b. In $\alpha Am_{mem}$ the helices form tight parallel interactions across the superhelical axis (Fig. 1c), creating a series of parallel dimeric helical pairs. Progressing along the superhelical axis, each dimer is rotated by –160°, creating a spiraling set of left-handed antiparallel helical pairs (Fig. 1a). The resulting up–up–down–down topology corresponds to class 5 packing in the amyloid classification scheme[23] (Supplementary Fig. 2). Both the parallel and antiparallel helical pairs have an approximately two-fold symmetry (Fig. 1c,d). Unlike in coiled coils, the helices are straight rather than curved around neighboring α-helices.

### Design of water-soluble cross-α spiral peptides.

There is considerable geometric complementarity in the side chain packing along the entire superhelical assembly of $\alpha Am_{mem}$. Each α-helix in the superhelix interacts in three geometrically distinct manners; namely, antiparallel interactions with helices within a sheet above and below the reference helix, as well as the parallel interaction across the fibril axis (Fig. 2a). Each of the three geometrically distinct helical pairs has left-handed crossing angles, which propagate to create the spiraling superhelix. Small alanine or serine residues (sticks in Fig. 2b) positioned on three faces of each α-helix appear to be critical for achieving the tight packing of the structure. They pack near the point of closest approach of each of the three helix–helix packing interfaces, where they facilitate close interhelical contacts; larger residues (sticks in Fig. 2b) line the interfaces as the helices diverge from a point of closest approach.

Although the dimers feature straight helices (rather than curving around one another), the packing shares similarities to knobs-into-holes packing of left-handed coiled coils near the point of closest approach. We therefore use the familiar heptad repeat nomenclature (Fig. 2c) to discuss packing of the helices. Ala17 facilitates a close contact between the parallel pairs of helices across the fibril axis in the $d$-$d'$ interface (defined in Fig. 2b), and Ser11 and Ala13 mediate close packing between the two geometrically distinct antiparallel helical pairings (Fig. 2b). Thus, the sequence of $\alpha Am_{mem}$ satisfies the requirements for mutual stabilization of three distinct packing arrangements of a single α-helix. Thus, the satisfaction of these multiple packing requirements underlies the tendency of the helices to remain

straight rather than coiling about one another (which would optimize packing about only one or two helix-helix interfaces in this scenario in which all helices have a left-handed crossing angle).

We used the abovementioned features to engineer the sequences of water-soluble peptides (Fig. 2d) capable of assembling into spiraling cross-α structures, as described in Methods. Briefly, the surface residues (Fig. 2e) in the $\alpha Am_{mem}$ structure were replaced with water-solubilizing Glu, Lys and Arg residues, which are capable of forming stabilizing electrostatic and hydrogen bonded interactions with the charged side chains (Fig. 2f). The remaining interior positions were retained as in $\alpha Am_{mem}$. To test the importance of the small Ser11 side chain in mediating interhelical interactions (Fig. 2d), we synthesized a set of peptides in which this residue was varied to a series of small residues—Gly, Ala and Ser—as well as a larger hydrophobic Leu side chain (Fig. 2d) in peptides designated $\alpha Am_G$, $\alpha Am_A$, $\alpha Am_S$ and $\alpha Am_L$, respectively.

## Assembly and crystal structures of αAm peptides.

The αAm peptides showed good solubility in deionized water but were found to assemble in a time-dependent manner when incubated in buffer at a broad range of pH from 3.5–9.5. The formation of amyloid is monitored by measuring the fluorescence enhancement of the fluorogenic dye thioflavin T (ThT), which is known to stain cross-α amyloid-like structures[14] and β-amyloid assemblies. Following dissolution in aqueous buffers, all of the αAm peptides showed time-dependent increases in the fluorescence intensity of ThT, with no apparent lag time in the kinetic traces (Fig. 3a). The toxic fibril-forming peptide PSMα3 has a similar aggregation behavior[14]. The half-time for assembly varied from approximately 7 min for the most hydrophobic peptide, $\alpha Am_L$, to 24 h for $\alpha Am_A$ (Fig. 3a). $\alpha Am_G$ showed relatively rapid kinetics ($t_{½}$ = 30 min), whereas $\alpha Am_S$ was slow ($t_{½}$ = 8 h), indicating that hydrophobicity alone does not explain the variation in the assembly kinetics. $\alpha Am_G$, $\alpha Am_A$ and $\alpha Am_S$ form thin fibrils as shown by negative-stain EM, whereas $\alpha Am_L$ forms much wider and longer fibrils (Fig. 3b). Infrared (IR) and circular dichroism (CD) spectroscopies were used to determine the secondary structure of the peptides. Each peptide showed a well-resolved spectrum, characteristic of the α-helix (Supplementary Fig. 3).

The peptides in Fig. 3b were crystallized, and high-resolution structures (Supplementary Table 1) were determined for all except $\alpha Am_A$, whose crystals diffracted to only 4.0 Å. The geometric parameters of the amyloid-like assemblies are listed in Supplementary Table 2. The superhelical structure of $\alpha Am_G$ was solved by molecular replacement in two space groups ($P4_322$, 2.49 Å resolution and $P6_122$, 3.30 Å resolution), and the structures were found to be nearly identical (0.4 Å Cα r.m.s. deviation computed over the 450 residues in the asymmetric unit (ASU)). There are nine parallel dimers in the ASU, which form a half turn of a superhelix (i.e., 18 parallel dimers/turn; pitch = 172.8 Å; Fig. 3c). The local packing interactions in the $\alpha Am_G$ structures are nearly identical to those in $\alpha Am_{mem}$, including the inclusion of small residues at positions where the helices approach most closely (Supplementary Fig. 4).

For $\alpha Am_S$, two superhelical arrangements were observed running in different directions through the crystal lattice: one had 20 parallel dimers/turn, whereas the other had 19.5

dimers/turn. $\alpha Am_S$ formed crystals in space group $P2_1$ (diffraction limit, 2.5 Å) with a large unit cell ($a$ = 161.166 Å; $b$ = 160.159 Å; $c$ = 198.502 Å), which presented a challenge for structure determination. Ultimately, the structure was solved by molecular replacement as described in Methods. The ASU contains 236 crystallographically nonequivalent straight α-helices. Together, they form three crystallographically distinct, but structurally related, superhelices. The first two superhelices (designated superhelices '1' and '2') have 20 dimers per turn (pitch = 198.5 Å; Fig. 3d). The remaining 78 parallel dimers form four complete turns of 'superhelix 3', which repeats over a length of 775.6 Å (19.5 parallel dimers per turn, pitch = 193.9 Å; Fig. 3e). Superhelix 3 can be conceptually subdivided into four subgroups, designated 3A–3D, each representing approximately one superhelical turn. A unit cell contains multiple copies of the subgroups, and subgroups 3A–3D stack between adjacent unit cells to generate the four turns in superhelix 3, which repeats through the crystal lattice (Supplementary Fig. 5). The small-residue packing patterns of $\alpha Am_S$ are very similar to those seen in $\alpha Am_{mem}$ (Supplementary Fig. 4), although the limited resolution of $\alpha Am_{mem}$ (3.5 Å) precluded a detailed comparison.

In summary, $\alpha Am_S$ and $\alpha Am_G$ have a limited degree of pitch diversity, ranging from 18 parallel dimers/turn, seen in two independent crystal structures for $\alpha Am_G$, to 19.5 and 20 dimers/turn, observed within a single crystal lattice for $\alpha Am_S$. Structurally, these changes represent only small differences in the crossing angle of the antiparallel helical pairs that define the superhelical pitch, ranging only slightly from 20° for $\alpha Am_G$ to 18°, 18° and 18.5° for the three superhelices 1, 2 and 3, respectively, observed for $\alpha Am_S$ (angles measured projected onto a plane normal to the superhelical axis). The minor increase in packing angle for $\alpha Am_G$ is likely related to differences in packing of the small Gly and Ser residues. Furthermore, electron density from one or more solvent molecules was observed between abutting Gly residues on adjacent helices in $\alpha Am_G$, although it could not be assigned with confidence at a diffraction limit of 2.5 Å.

More deep-seated structural differences were seen in two variants, which we synthesized to evaluate the effect of small-to-large variations at the packing interface; the variants $\alpha Am_L$ and $\alpha Am_F$ have a large Leu and an even larger Phe side chain at position 11, respectively, while all three critical small positions at 11, 13 and 17 were simultaneously changed to Leu in $\alpha Am_{3L}$ (Fig. 2d). $\alpha Am_F$ and $\alpha Am_{3L}$ were helical in solution (Supplementary Fig. 3) but had limited solubility in buffers and failed crystallization attempts, and were observed to form amorphous aggregates by negative-stain EM (Supplementary Fig. 6); they therefore were not studied further. By contrast, $\alpha Am_L$, in which only one small residue at position 11 was mutated to intermediate-sized leucine, rapidly assembled into a structure that bound ThT (Fig. 3a) and formed crystals that diffracted to 2.0 Å (Supplementary Table 1). Interestingly, the peptide adopts an entirely different structure from the other peptides with small residues at this position (Fig. 4a). The large Leu side chain apparently disrupts the cross-α packing, and instead defaults to form a *canonical* antiparallel four-helix coiled coil[24] (Fig. 4b). The structure of $\alpha Am_L$ can be related to that of $\alpha Am_S$ by a 48° rotation of the α-helices about their α-helical axes and an approximately 5-Å net translation of the parallel helices, such that they come to occupy more distant diagonal positions in the four-helix bundle (Fig. 4b). These geometric changes place the small Ala residues at positions 13 and 17 into "*d*" and "*a*" positions of a heptad repeat, respectively (Supplementary Fig. 7a,b). In

the tetramer, these small residues pack together with larger residues in a geometrically complementary jigsaw-puzzle-like manner similar to that first seen in the protein ROP[25].

The $\alpha Am_L$ tetramers were found to form a much more open and wide helical polymer rather than a cross-α amyloid-like structure. The large Leu11 side chains project from the surface of the bundle, where they mediate hydrophobic lateral contacts between individual tetramers (Fig. 4a). To probe the role of Leu11 and other hydrophobic residues at the tetramer–tetramer interface in mediating its higher-order assembly, we converted the apolar residues that facilitate the assembly to polar side chains while maintaining the identities of the remaining residues (Fig. 2d and Supplementary Fig. 7c,d). The crystal structure of this peptide, designated αTet, was nearly identical to the tetrameric unit of $\alpha Am_L$ (Cα r.m.s. deviation 0.7 Å over the full tetramers). However, αTet did not show a higher-order assembly in solution as assessed by the ThT assay (Fig. 3a). Furthermore, there were few intertetramer contacts in the lattice, and those that were formed were primarily solvent mediated (Supplementary Fig. 8).

### Association of αAm peptides in mammalian cells.

The aggregation of amyloid-forming proteins such as tau and α-synuclein in mammalian cells is often assessed by fluorescence microscopy, using genetically encoded fusions of the protein of interest and a fluorescent protein[26,27]. The formed protein inclusions appear as bright intracellular puncta and are accompanied by the loss of the more diffuse staining from soluble proteins (Supplementary Fig. 9a). To determine whether the α Am series of peptides similarly formed intracellular inclusions, we tagged four peptides ($\alpha Am_G$, $\alpha Am_A$, $\alpha Am_S$ and $\alpha Am_L$) with enhanced GFP (EGFP) and expressed them in HEK 293 T cells. All of these αAm peptides aggregated in the cytosol as assessed from the presence of bright puncta (diameter < 5 μm; Fig. 5a). To pinpoint the physical properties of the inclusions, we performed fluorescence recovery after photobleaching (FRAP) experiments, which examine protein motility in the inclusions (Fig. 5b). Interestingly, both $\alpha Am_G$ and $\alpha Am_S$, which had been shown by crystallography to form cross-α structures, displayed irreversible photobleaching over a period of 10 min (during which time the fluorescence intensity of the bleached area stayed below 50% of prebleach level). The results suggest that the fusion proteins in the inclusions are immobile within this time range (Fig. 5b). The α $Am_A$ fusion, which presumably also forms a cross- α spiral (given the similarity of its sequence to those of $\alpha Am_G$ and $\alpha Am_S$), behaved similarly. In contrast, $\alpha Am_L$-expressing cells showed almost fully recovered fluorescence, indicating that this protein is mobile in the puncta structure (Supplementary Fig. 9b). The result suggests that this peptide forms liquid droplet-like phases in the cells, which is consistent with the more open and less tightly packed helical polymer formed by this peptide. As a negative control, there is no puncta in α Tet-expressing cells (Supplementary Fig. 10).

## Discussion

Molecular assembly of peptides and proteins is used throughout biology for compartmentalization and display purposes. Protein design provides an approach to test and extend our understanding of assembly and to engineer artificial molecules that can directly

assemble with precisely defined stoichiometries and spacing. For example, principles have been developed for the design of self-assembled coiled coils, which can be used to test the role of dimerization or oligomerization in diverse cellular processes[28,29]. Much larger polymeric assemblies are also ubiquitous throughout nature, and they range from the very rigid, precisely ordered and closely spaced spiral arrays formed by amyloid-forming sequences to highly mobile liquid droplet-like phases[30]. Here, we describe the design of two types of self-assembling systems: densely packed cross- α amyloid-like materials as well as a less densely packed reversibly assembling helical polymer. Both might prove useful for diverse applications from nanotechnology to cell biology, where they could provide useful modules for inducing assembly of protein domains into well-defined and predetermined arrays.

The spiraling cross-α amyloid-like conformation is particularly interesting, as to the best of our knowledge it had not been crystallographically characterized in natural or synthetic systems. Its conformation contrasts with the more planar bilayer-like packing arrangement seen in designed helical peptides[15,16] and a natural toxic peptide[14] (Supplementary Fig. 11a). The features required for assembly into this cross-α amyloid-like spiral structures are relatively simple: small residues positioned on three faces of an α-helix mediate close contacts with neighboring helices (Fig. 2 and Supplementary Fig. 4). Together with larger apolar residues aligned along the three packing interfaces, the small residues mediate packing between straight helices with a small (15° to 20°) left-handed crossing angle. The uniform left-handed crossings give rise to a progressive left-handed screw that generates the spiraling amyloid-like structures (Supplementary Fig. 11b). Meanwhile, it is interesting to compare the helical polymer structure of $\alpha Am_L$ to that of the SAM oligomerization domain[31] (Supplementary Fig. 11c), which is a widely used oligomerization motif for assembling a variety of domains for diverse signaling functions[32,33]. Disruption of this packing motif by increasing the bulk of even one of the small residues in $\alpha Am_L$ resulted in the formation of classical antiparallel four-helix bundles that assembled in a less regular and dense manner through association of the faces of tetrameric units (Supplementary Fig. 11d). Thus, the folds described in this work provide a range of assemblies that have not yet been discovered in nature. Furthermore, these folds potentially provide both packing densities and the ability to direct patterned linear arrays of fused domains that aptly reflect phenomena found in nature.

## Methods

### Protein design.

The sequences of water-soluble αAm peptides were designed on the basis of the crystal structure of $\alpha Am_{mem}$. The residues on the positions *b*, *c* and *f* in the heptad repeats as shown in Fig. 2c were designed with the models generated by the Rosetta fixbb module[34], and residues on other positions are fixed. The residues on positions *b*, *c* and *f* allowed only charged residues Arg, Asp, Lys or Glu. Rosetta-generated models were used to discover combinations that could form interchain hydrogen bonds, and we then manually selected pairs for the final sequence of $\alpha Am_S$. The sequences of $\alpha Am_G$, $\alpha Am_A$ and $\alpha Am_L$ were obtained by changing the residues on position *e* to modulate the interface size. The sequence

of $\alpha Am_{3L}$ is based on that of the water-soluble αAm peptides for a systematic change of all three small residues to test their importance. The sequence of αTet is obtained by manually changing the residues at positions *c* and *e* in the heptad designation for the antiparallel tetramer subunit of $\alpha Am_L$ for intrachain hydrogen bonds between the residues i→i + 2 and i→i + 3.

### Peptide synthesis and purification.

The peptides were synthesized and purified according to the procedures previously described[22].

### Thioflavin-T kinetics assay.

The peptides were prepared to a final volume of 100μL at a final concentration of 200μM peptides and 200μM ThT in 1× PBS in the 96-well bottom-clear nonbinding plates (Greiner). Each peptide was tested with four replicates. The plate was sealed with a clear film (Nunc), placed in a Spectramax M5 plate reader (Molecular Devices) set at 37°C, and subjected to repeated rounds of 1-min rest and 4-min shaking. The reading of the ThT fluorescence was top-read at $\lambda_{ex}$ = 444 nm and $\lambda_{em}$ = 485 nm and recorded in an intervals of 5 min for 96 h.

### Formation of fibrils.

The peptides were prepared at 100μM in 1× PBS in 1.5-mL Eppendorf tubes. Samples were incubated at 37°C for 96 h under constant agitation at 900 r.p.m.

### Negative-stain electron microscopy.

A suspension of 5μL samples prepared as described above was briefly vortexed and then applied to 300 mesh Cu grids coated with thin carbon and incubated for ~20 min. Following sample incubation, the grids were stained twice with uranyl formate (for $aAm_G$) or uranyl acetate (for other peptides). The excess stain was removed by blotting from the side and vacuum dried. Prepared grids were imaged with a FEI TECNAI 20 operated at 200 kV. Images were recorded using an 8k × 8k TemCam-F816 CMOS camera from TVIPS at a magnification of 11,000× ($\alpha Am_L$), 62,000× ($\alpha Am_G$, $\alpha Am_A$, and $\alpha Am_s$) and 29,000× ($\alpha Am_F$ and $\alpha Am_{3L}$) with −1.5 μm defocus.

### Infrared spectroscopy.

5 μL of the fibril solution was slowly dried onto a ZnSe single reflection ATR crystal plate for the Smart iTX optical module of the Thermo Fisher Nicolet iS10 FTIR spectrometer. For each spectrum, 500 scans were taken at room temperature (22–25 °C) with a nominal spectral resolution of 4 $cm^{-1}$. The ATR crystal was previously cleaned with water and isopropanol.

### Circular dichroism spectroscopy.

CD spectra of 40μM peptides dissolved in PBS buffer were collected at room temperature using a Jasco J-810 CD and 1 mm path-length cuvettes. The spectra were collected after dilution from de-ionized water into buffer.

### Crystallography.

The peptide αAm$_{mem}$ was dissolved at 5 mg/mL in 50 mM octyl-β-glucoside in water, and other water-soluble peptides were dissolved at 10–15 mg/mL in water. The hanging-drop vapor-diffusion method at room temperature was used for crystallization. The crystallization conditions for the different peptides are as follows: (1) αAm$_{mem}$: 35% MPD, 0.2 M $MgCl_2$ and imidazole 0.1 M pH 8; (2) αAmG (#1): 0.2 M ammonium acetate, 0.1 M trisodium citrate pH 5.6, 30% (w/v) MPD; (3) αAmG (#2): 40% MDP, 0.2 M K/Na tartrate; (4) αAm$_A$: 45% MPD, 0.25 M $NaH_2PO_4$; (5) αAm$_S$: 45% MPD, 0.2 M Na formate; (6) αAm$_L$: 45% MPD, 0.6 M $NaH_2PO_4$; (7) αTet: 2.0 M Na formate, 0.1 M Na acetate. Crystals were flash frozen with liquid $N_2$, and data collection temperature was 100 K. No extra/additional cryoprotectant was required for the peptides except αTet, for which 30% glycerol was used. The data of αAm$_{mem}$, αAm$_G$ and αTet were collected at the Advanced Light Source, Lawrence Berkeley National Laboratory at the Beamline 8.3.1 on a Pilatus3 6 M detector with X-ray wavelength of 1.11584 Å. Those for αAm$_A$, αAm$_S$, αAm$_L$ and αAm$_L$-2 were recorded on a Pilatus3 6 M detector with a wavelength of 1.03320 Å at the Beamline 23ID-D of the Argonne National Laboratory. Data were processed with HKL2000 (ref. [35]) and/or XDS[36] packages. Statistics for data processing and structural refinement were shown in Supplementary Table 1.

A molecular replacement method was used to solve the structures. COOT[37] was used for modeling and rebuilding. For αAm$_{mem}$, a single helix of the $Zn^{2+}$-binding helical bundle 4EH1 (ref. [22]) (PDB code 5WLJ) was truncated to a polyalanine search model; the searching was done with Phaser[38]. In total, eight copies of helices were located in the asymmetric unit. In contrast to the antiparallel bundles of 4EH1, however, the peptides were stacked by alternately reversed parallel helical pairs. Due to low resolution, the orientations of helices were determined by refinement with different combinations of helical directions; difference Fourier analyses and identification of the interaction between polar residues from neighboring chains played key roles in removal ambiguity. Similarly, for αAm$_L$, the same single helix was used as search model, and all four helices were located with Phaser[38]; the αAm$_L$ subunit appeared to be antiparallel bundles, similarly to that in 4EH1. A similar strategy was applied to solving and refining the structure of αTet. These structures were refined with REFMAC[39] in the CCP4 packages[40] or Phenix[41].

For αAm$_S$, the molecular replacement was challenging because there was calculated to be ~332 copies of the αAmS peptides in the asymmetric unit, assuming 50% solvent content in the unit cell. Helical dimers from 4EH1 and the four-helix bundle from 4EH1 were used to discover potential orientations within the large unit. During the molecular replacement test, among the random outputs, very occasionally, solutions were observed in which two bundles were docked with a relative rotation of ~30–40 degrees along the primary noncrystallographic symmetry (NCS) axis (parallel to cell edge *c*, calculated by self-rotation function with MOLREP in CCP4 (ref. [40])). However, the NCS-fold was hard to assign, and the distance between these two bundles varied from 18 to 25 Å. The NCS-fold was shown to be compatible with possible numbers from 2 to 12, or even higher, owing to too many molecules in the asymmetric unit. However, the strong NCS signal along *c* enabled us to rationally scan potential molecular packing in this direction. To facilitate the calculation, the

monoclinic unit cell was first re-indexed to switch the *a* and *c* axes. Molecular replacement was then redone to acquire the same aforementioned "dimer" (dimer of four-helix bundles) with the rotational NCS along the new "*a*" direction. Thereafter, a single four-helical bundle of the "dimer" was translated and fixed at the unit-cell origin. A more sophisticated dimeric model was then generated by expanding the model from the first bundle by rotating a 360/*n* degree (*Chi* angle in Polar angle convention) plus a translation of ±*a*/(*n***k*) (*a* is the cell constant of the new "*a*"; *n* is the postulated NCS-fold; *k* is an integer that keeps *a*/(*n***k*) in the reasonable interaction distance of two four-helical bundles and restricts *a*/(*n***k*) in the range of 15–25 A). When one direction is fixed as the primary NCS direction for expanding model along the new "a" axis, two other directions (denoted by two other polar angles, *Phi* and *Psi*) of the first placed bundle at origin were scanned in ± 5 degrees with 1-degree intervals, and this scanning was incorporated into the model expansion and molecular replacement test. The best dimeric model was found with $n = 10$, i.e., the two bundles were related by 36 degrees along the new "*a*" and a distance of 19.85 Å. After this, further elongating the model to a string of 5 bundles (still antiparallel $\alpha Am_L$) resulted in the discovery of 20 bundles with MOLREP; each 10 bundles in a string were exactly fit into a unit distance of the new "*a*". The 10-bundle was then used as model, and four extra 10-bundles were found (with one bundle overlapped in total). Overall, in total 59 four-helical bundles, or 236 helices, were replaced in the ASU. After all peptides were placed in ASU, the cells was re-indexed back to the original unit cell convention by switching "*a*"/"c" again, and the coordinates were transformed accordingly. During refinement, half of the helices were revealed to be reversed and were corrected. During the refinement thereafter, the NCS was turned off, as a 236-fold of NCS simply slowed down the refinement for more than 10 folds. Rigid body and TLS domains were reduced down to single helices. The refinement was performed with PHENIX[41] for its great advantage in handling 236 chains.

For the $\alpha Am_G$ ($P4_322$ space group), the molecular replacement was started with the antiparallel $\alpha Am_L$ bundle as model too (in parallel to the $\alpha Am_S$ project). In total, 4.5 bundles (18 helices) were found. Similarly, half of the $\alpha Am_G$ were revealed to be reversed. The refinement was done with REFMAC[39]. For the $aAm_G$ in another space group ($P6_122$), the previous solution (18 peptides) was used as model, and exactly the same peptide content was located in the asymmetric unit. The refinement strategy was similarly used as mentioned above.

For $\alpha Am_A$, the data were constantly restricted to ~4.0 Å. Difficulty persists when removing the huge bias and ambiguity of MR solutions, and we are struggling for data of better quality.

### Cellular assay.

Each αAm peptide was cloned into a pcDNA3-EGFP vector containing EGFP. The sequence of each αAm peptide was inserted at the 3' end of EGFP gene with a long flexible linker containing Gly, Ala and Ser repeats (GSGSA GGSAGGSAGGSAGGSAGGSAGGS). The fusion proteins (EGFP-linker-α Am) were expressed in HEK 293 T cells by transient transfection. HEK 293 T cells were transfected 48 h before imaging and photobleaching. UV light (405 nm) was applied at 80% power to each sample at 20×. Samples were illuminated

for 1,300 ms to bleach GFP fluorescence in the regions of interest (ROIs). All samples were imaged for two frames before photobleaching, and were monitored afterwards for 10 min with a 5-s interval. Images were captured by an Olympus FV3000 inverted confocal laser scanning microscope. The intensity of 488 nm fluorescence in ROIs (with background fluorescence subtracted) was measured using NIH ImageJ.

Values in Supplementary Fig. 9b were plotted as percentage of the first frame before photobleaching.

### Statistics.

Experiments on the ThT-binding kinetics assay, negative-stain EM, and IR and CD spectroscopies were repeated two times with similar results. In the ThT-binding kinetics assay, four technical replicates were used for averages and standard errors. At least five images were taken for each reported peptide by negative-stain EM. The cellular fluorescence and photobleaching experiments were independently repeated three times with similar results. For each reported peptide, at least five images were taken for the cellular fluorescence observation and at least six puncta were used for time-lapse photobleaching recording.

## Supplementary Material

Refer to Web version on PubMed Central for supplementary material.

## Acknowledgements

We thank D. Bulkley, P. Jin, S. Li, X. Liu, N. Polizzi, N. Schmidt and H. Wu for technical help. This work was primarily supported by NIH grant R35GM122603 to W.F.D., with additional support from the NSF (CHE1413295) for the MRSEC program to the LRSM at the University of Pennsylvania. H.T.K. was supported by a Ruth L. Kirschstein NRSA Postdoctoral Fellowship (F32GM125217). Y.L. was supported by a Howard Hughes Medical Institute-Helen Hay Whitney Foundation Postdoctoral Fellowship.

## References

1. Gazit E Self-assembled peptide nanostructures: the design of molecular building blocks and their technological utilization. Chem. Soc. Rev. 36, 1263–1269 (2007). [PubMed: 17619686]
2. Shigemitsu H & Hamachi I Design strategies of stimuli-responsive supramolecular hydrogels relying on structural analyses and cell-mimicking approaches. Acc. Chem. Res. 50, 740–750 (2017). [PubMed: 28252940]
3. Shu JY, Panganiban B & Xu T Peptide-polymer conjugates: from fundamental science to application. Annu. Rev. Phys. Chem. 64, 631–657 (2013). [PubMed: 23331303]
4. Riek R & Eisenberg DS The activities of amyloids from a structural perspective. Nature 539, 227–235 (2016). [PubMed: 27830791]
5. Prusiner SB Cell biology. A unifying role for prions in neurodegenerative diseases. Science 336, 1511–1513 (2012). [PubMed: 22723400]
6. Sacchettini JC & Kelly JW Therapeutic strategies for human amyloid diseases. Nat. Rev. Drug Discov. 1, 267–275 (2002). [PubMed: 12120278]
7. Toyama BH & Weissman JS Amyloid structure: conformational diversity and consequences. Annu. Rev. Biochem. 80, 557–585 (2011). [PubMed: 21456964]
8. Knowles TP & Buehler MJ Nanomechanics of functional and pathological amyloid materials. Nat. Nanotechnol. 6, 469–479 (2011). [PubMed: 21804553]

9. Rufo CM et al. Short peptides self-assemble to produce catalytic amyloids. Nat. Chem. 6, 303–309 (2014). [PubMed: 24651196]
10. Makhlynets OV, Gosavi PM & Korendovych IV Short self-assembling peptides are able to bind to copper and activate oxygen. Angew. Chem. Int. Edn Engl. 55, 9017–9020 (2016).
11. Tena-Solsona M et al. Emergent catalytic behavior of self-assembled low molecular weight peptide-based aggregates and hydrogels. Chemistry 22, 6687–6694 (2016). [PubMed: 27004623]
12. Friedmann MP et al. Towards prebiotic catalytic amyloids using high throughput screening. PLoS One 10, e0143948 (2015).
13. Childers WS, Ni R, Mehta AK & Lynn DG Peptide membranes in chemical evolution. Curr. Opin. Chem. Biol. 13, 652–659 (2009). [PubMed: 19879180]
14. Tayeb-Fligelman E et al. The cytotoxic Staphylococcus aureus PSMα3 reveals a cross-α amyloid-like fibril. Science 355, 831–833 (2017). [PubMed: 28232575]
15. Privé GG, Anderson DH, Wesson L, Cascio D & Eisenberg D Packed protein bilayers in the 0.90 A resolution structure of a designed alpha helical bundle. Protein Sci. 8, 1400–1409 (1999). [PubMed: 10422828]
16. Patterson WR, Anderson DH, DeGrado WF, Cascio D & Eisenberg D Centrosymmetric bilayers in the 0.75 A resolution structure of a designed alpha-helical peptide, d,l-Alpha-1. Protein Sci. 8, 1410–1422 (1999). [PubMed: 10422829]
17. Egelman EH et al. Structural plasticity of helical nanotubes based on coiled-coil assemblies. Structure 23, 280–289 (2015). [PubMed: 25620001]
18. Brunette TJ et al. Exploring the repeat protein universe through computational protein design. Nature 528, 580–584 (2015). [PubMed: 26675729]
19. Main ER, Jackson SE & Regan L The folding and design of repeat proteins: reaching a consensus. Curr. Opin. Struct. Biol. 13, 482–489 (2003). [PubMed: 12948778]
20. Plückthun A Designed ankyrin repeat proteins (DARPins): binding proteins for research, diagnostics, and therapy. Annu. Rev. Pharmacol. Toxicol. 55, 489–511 (2015). [PubMed: 25562645]
21. Joh NH et al. De novo design of a transmembrane Zn2+-transporting four-helix bundle. Science 346, 1520–1524 (2014). [PubMed: 25525248]
22. Zhang S-Q et al. De novo design of tetranuclear transition metal clusters stabilized by hydrogen-bonded networks in helical bundles. J. Am. Chem. Soc. 140, 1294–1304 (2018). [PubMed: 29249157]
23. Eisenberg DS & Sawaya MR Structural studies of amyloid proteins at the molecular level. Annu. Rev. Biochem. 86, 69–95 (2017). [PubMed: 28125289]
24. Szczepaniak K, Lach G, Bujnicki JM & Dunin-Horkawicz S Designability landscape reveals sequence features that define axial helix rotation in four-helical homo-oligomeric antiparallel coiled-coil structures. J. Struct. Biol. 188, 123–133 (2014). [PubMed: 25278129]
25. Banner DW, Kokkinidis M & Tsernoglou D Structure of the ColE1 rop protein at 1.7 A resolution. J. Mol. Biol. 196, 657–675 (1987). [PubMed: 3681971]
26. Sanders DW et al. Distinct tau prion strains propagate in cells and mice and define different tauopathies. Neuron 82, 1271–1288 (2014). [PubMed: 24857020]
27. Prusiner SB et al. Evidence for α-synuclein prions causing multiple system atrophy in humans with parkinsonism. Proc. Natl. Acad. Sci. USA 112, E5308–E5317 (2015). [PubMed: 26324905]
28. Thompson KE, Bashor CJ, Lim WA & Keating AE SYNZIP protein interaction toolbox: in vitro and in vivo specifications of heterospecific coiled-coil interaction domains. ACS Synth. Biol. 1, 118–129 (2012). [PubMed: 22558529]
29. Fletcher JM et al. A basis set of de novo coiled-coil peptide oligomers for rational protein design and synthetic biology. ACS Synth. Biol. 1, 240–250 (2012). [PubMed: 23651206]
30. Banani SF, Lee HO, Hyman AA & Rosen MK Biomolecular condensates: organizers of cellular biochemistry. Nat. Rev. Mol. Cell Biol. 18, 285–298 (2017). [PubMed: 28225081]
31. Kim CA, Sawaya MR, Cascio D, Kim W & Bowie JU Structural organization of a Sex-comb-on-midleg/polyhomeotic copolymer. J. Biol. Chem. 280, 27769–27775 (2005). [PubMed: 15905166]

32. Kim CA & Bowie JU SAM domains: uniform structure, diversity of function. Trends Biochem. Sci. 28, 625–628 (2003). [PubMed: 14659692]

33. Wu H & Fuxreiter M The structure and dynamics of higher-order assemblies: amyloids, signalosomes, and granules. Cell 165, 1055–1066 (2016). [PubMed: 27203110]

34. Kuhlman B & Baker D Native protein sequences are close to optimal for their structures. Proc. Natl. Acad. Sci. USA 97, 10383–10388 (2000). [PubMed: 10984534]

35. Otwinowski Z & Minor W Processing of X-ray diffraction data collected in oscillation mode. Methods Enzymol. 276, 307–326 (1997).

36. Kabsch W Integration, scaling, space-group assignment and post-refinement.Acta Crystallogr. D Biol. Crystallogr. 66, 133–144 (2010).

37. Emsley P, Lohkamp B, Scott WG & Cowtan K Features and development of Coot. Acta Crystallogr. D Biol. Crystallogr. 66, 486–501 (2010). [PubMed: 20383002]

38. McCoy AJ et al. Phaser crystallographic software. J. Appl. Crystallogr. 40, 658–674 (2007). [PubMed: 19461840]

39. Murshudov GN et al. REFMAC5 for the refinement of macromolecular crystal structures. Acta Crystallogr. D Biol. Crystallogr. 67, 355–367 (2011). [PubMed: 21460454]

40. Winn MD et al. Overview of the CCP4 suite and current developments. Acta Crystallogr. D Biol. Crystallogr. 67, 235–242 (2011). [PubMed: 21460441]

41. 41 Adams PD et al. PHENIX: a comprehensive Python-based system for macromolecular structuresolution. Acta Crystallogr. D Biol. Crystallogr. 66, 213–221 (2010)).. [PubMed: 20124702]

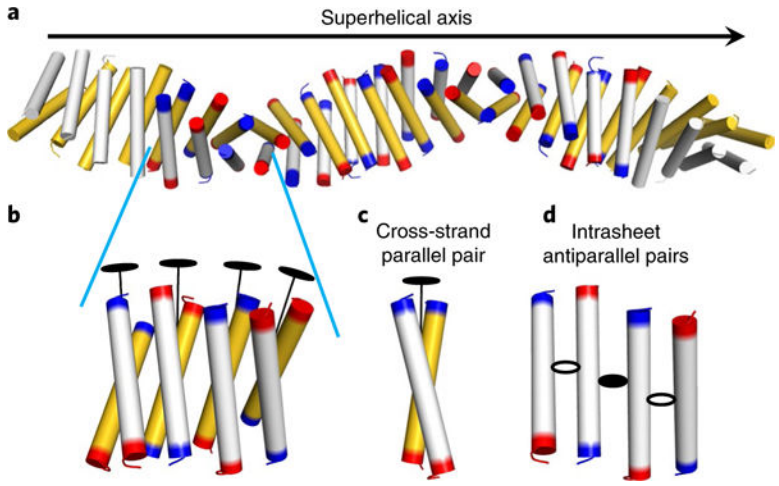


**Fig. 1 |. The amyloid-like structure of αAm$_{mem}$.**

**a**, The superhelical repeat consists of 16 dimers, which are colored blue and red at the N- and C-termini, respectively. The helix dimer subunits progress perpendicularly to the superhelical axis. **b**, The crystallographic asymmetric unit consists of two twisted sheets of helical dimers, which are colored white and golden. **c**, The basic unit of the whole amyloid-like assembly is a pseudo-two-fold symmetric cross-strand parallel helix dimer, with two-fold rotational axis running along the long axis of the dimer indicated by a black oval and line. **d**, In each sheet, there are two different types of two-fold symmetric antiparallel helix pairs (shown in more detail in Fig. 2). These pairs have approximately two-fold symmetry, but this time with the two-fold symmetry axis directed between the helices as indicated by open and solid ovals. Note that the noncrystallographic pseudosymmetry axes shown in **b-d** are all directed orthogonally to the main superhelical axis of the overall structure shown in **a**.

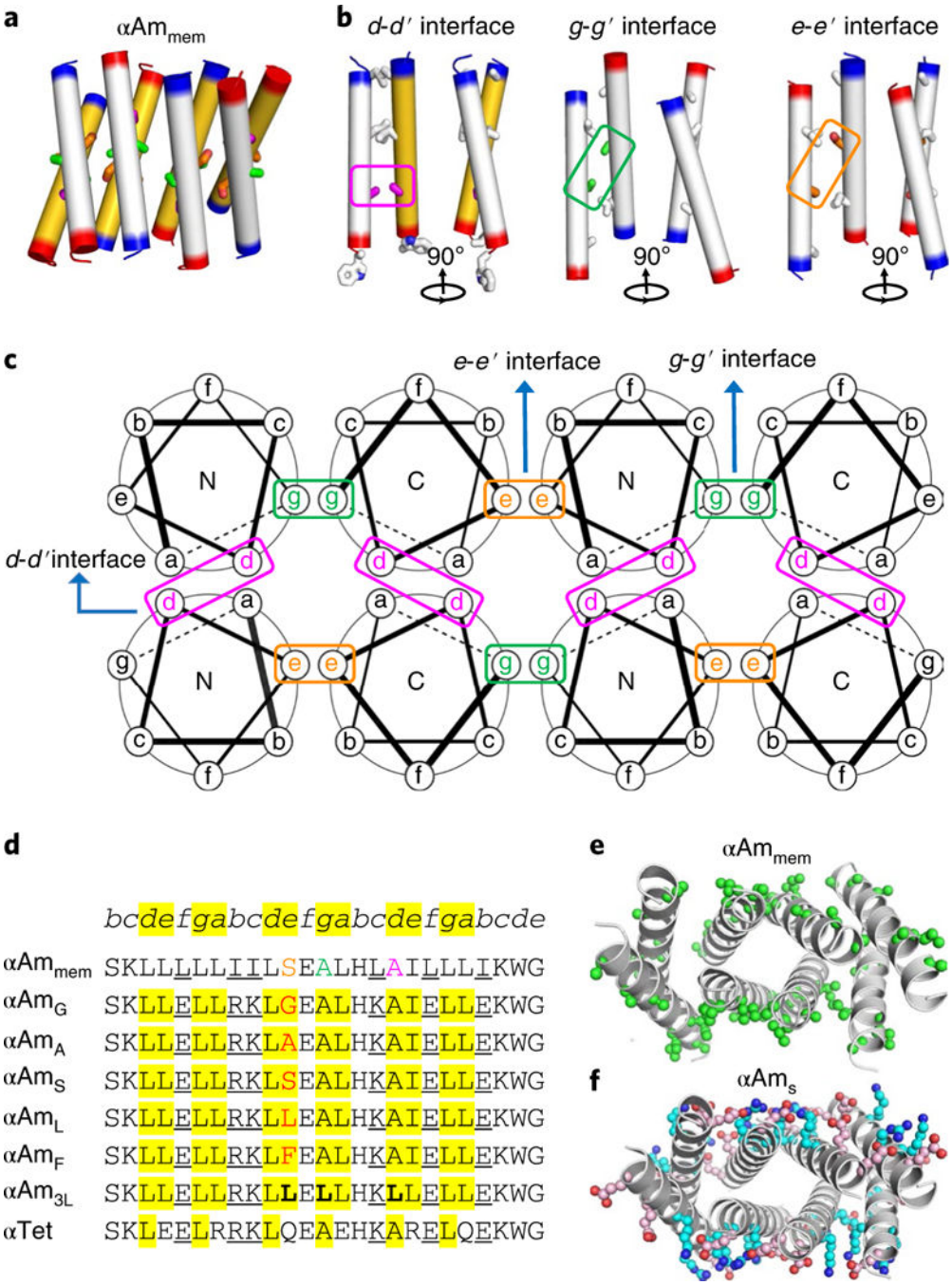


**Fig. 2 |. Design of cross-α amyloid-like assembly.**

**a**, Three types of helix–helix interfaces with small-residue (as sticks) packing exist in the αAm$_{mem}$ amyloid-like structure. **b**, Ala17 (magenta), Ala13 (green) and Ser11 (carbon colored orange) as small residues are involved in the interhelical packing with larger hydrophobic residues (carbon as white sticks) occurring at positions filling the space as the helices diverge from the point of closest approach near the small residues. **c**, Their interfaces are designated as *d-d′*, *g-g′* and *e-e′* interfaces, according to the helix wheels for the amyloid-like structure with a parallel dimer as the subunit (the orientation of the N- versus

C-terminus toward the viewer is denoted as N and C, respectively). The small residues and the corresponding interfaces in the helix wheels are boxed in **b** and **c**, respectively. **d**, The designed sequences intended to form water-soluble amyloid-like structures is compared to $\alpha Am_{mem}$. **e,f**, The sequence changes between the crystal structures of $\alpha Am_{mem}$ (**e**) vs. $\alpha Am_S$ (**f**) in ball-and-stick representation. Their sequences are designed by keeping the residues at the hydrophobic core intact, but modifying the residues (underlined positions) facing the solvent with charged residues for enhanced electrostatic and hydrogen bonded interactions. The hydrophobic residues on the surface of $\alpha Am_{mem}$ are colored green, whereas the designed charged residues at the same locations of $\alpha Am_S$ are colored cyan and pink for positively and negatively charged, respectively. As shown in **d**, the residue on position 11 in the *e*-*e*′ interface is varied to examine its size effect, as shown in red in $\alpha Am_G$, $\alpha Am_A$ $\alpha Am_S$, $\alpha Am_L$ and $\alpha Am_F$. The synergistic effects of varying three small residues (bolded in **d**) to Leu are tested by $\alpha Am_{3L}$. A nonaggregating water-soluble αTet is also designed.

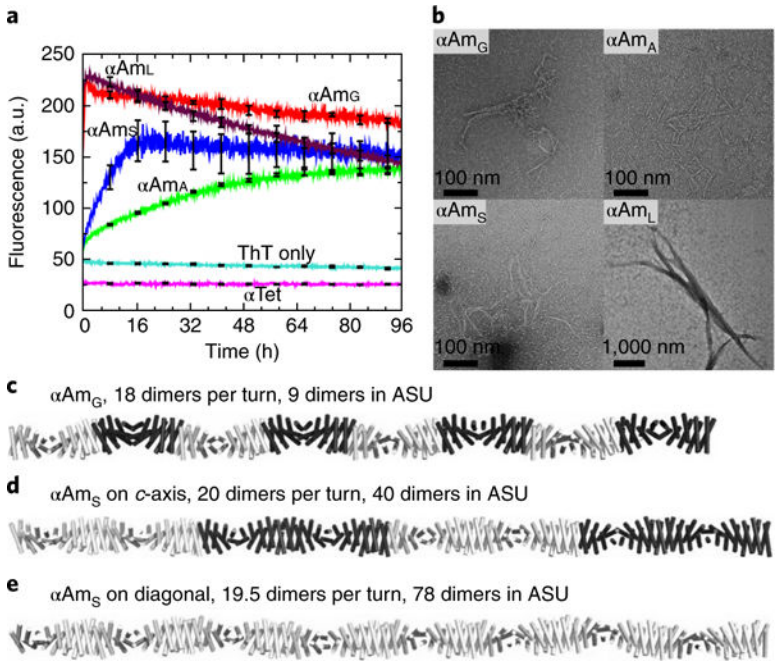


**Fig. 3 |. The aggregation behavior and fibril formation of the water-soluble peptides and the crystal structures of the cross-α amyloid-like fibrils.**

**a**, Aggregation kinetics of the peptides monitored by ThT fluorescence. The s.e.m. of n = 4 technical replicates are shown by error bars. **b**, Negative-stain EM images of the fibrils formed by the designed peptides αAmG, αAmA, αAmS, and αAmL. EM was repeated twice independently with similar results. c-e, Four turns of the αAmG (**c**), αAmS on the crystallographic c-axis (**d**) and αAmS on the diagonal (**e**) in the unit cell. In c eight repeats of the peptide assembly of αAmG in the asymmetric unit (ASU) are shown; in **d** four repeats of 20 dimers of αAmS on the c-axis are shown; in **e** a single repeat of 78 dimers on the diagonal in the ASU is shown.

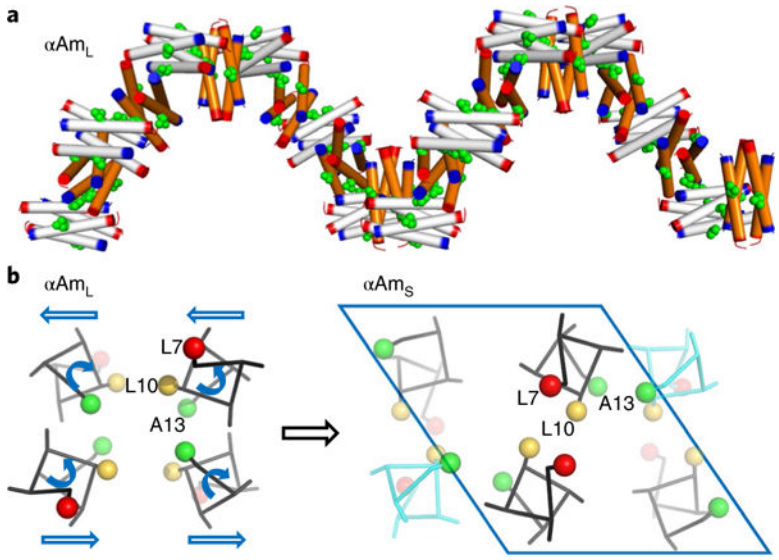


**Fig. 4 |. Packing of αAm$_L$ as a helical polymer composed of helix tetramers and its configurational relationship with the cross-α amyloid-like assembly of αAm$_G$ and αAm$_S$.**

**a**, Two turns of αAm$_L$ superhelices; the N- and C-termini of the peptides are colored blue and red, respectively, and the side chain of Leu11 is colored green. The helical tetramer subunits are colored white and orange alternately. **b**, The geometric relationship between the structure of an αAm$_L$ tetramer and the cross-α spiral of αAm$_S$. The left panel shows a slice of the crystal structure of αAm$_L$, which forms a canonical four-helix bundle that assembles into the helical polymer shown in **a**. Thus, the repeating unit αAm$_L$ is a tetramer instead of the parallel dimer seen in αAm$_S$. The tetramer of αAm$_L$ can be converted to the repeating structure of αAm$_S$ by the indicated rotations of the helices in αAm$_L$ by 48° and the translation of the helices by approximately 5Å as indicated. In both αAm$_L$ and αAm$_S$, the balls in red, yellow and green are residues Leu7, Leu10 and Ala13, respectively. The two helices uninvolved in configurational transformation in αAm$_S$ are colored cyan.

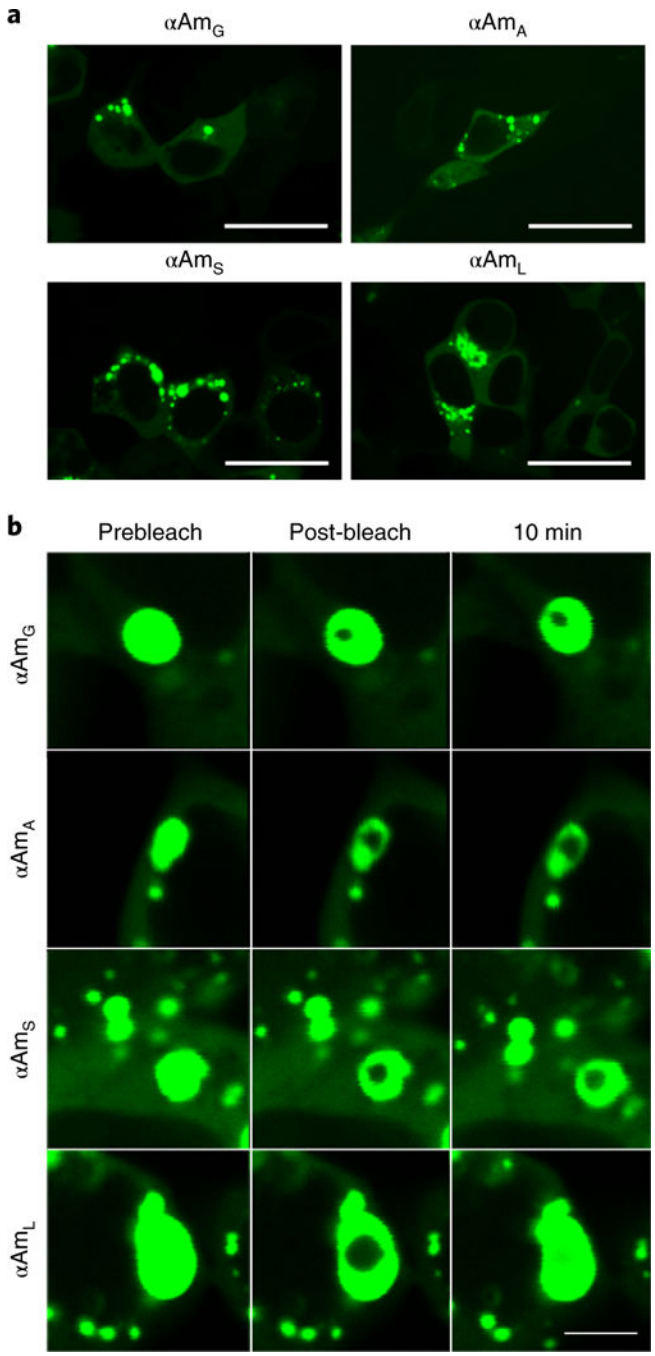


**Fig. 5 |. EGFP-tagged α Am peptides form inclusions in the cytosol of mammalian cells; αAm$_G$, αAm$_A$ and αAm$_S$ form a solid-like phase, whereas αAm$_L$ is more mobile.**

**a,** Fluorescence images of HEK 293 T cells expressing EGFP-fused α Am peptides. Scale bars, 50 μm. **b**, Confocal images show droplets of αAm$_G$, αAm$_A$, αAm$_S$ and αAm$_L$ in HEK 293 T cells before and after photobleach. Scale bar, 5 μm. These experiments were repeated independently three times with similar results.